PROCEEDINGS, 45th Workshop on Geothermal Reservoir Engineering
Stanford University, Stanford, California, February 10-12, 2020
SGP-TR-216

Study of Foam Fracturing for Enhanced Geothermal Systems Using Model Material[a]

Hong Wang[1,*], Jy-An J. Wang[1], Yarom Polsky[2], Fei Ren[3], Haoqi Li[3], Viren Thakore[3], Jiaxin Xi[3]

[1]Materials Science & Technology Division, Oak Ridge National Laboratory, PO Box 2008, MS 6069, Oak Ridge, TN 37831

[2]Electrical & Electronics Systems Research Division, Oak Ridge National Laboratory, PO Box 2008, MS 6075, Oak Ridge, TN 37831

[3]Temple University, 1947 North 12th Street, Philadelphia, PA 19122

*Corresponding Author. E-mail: wangh@ornl.gov

Keywords: foam fracturing, pulsed injection, waterless, EGS stimulation, cement

ABSTRACT

Foam fracturing is considered a potential approach to address water concerns with hydraulic fracturing in the development of enhanced geothermal systems (EGS). In many EGS sites, water required for hydraulic fracturing is either unavailable, extremely costly or environmentally unsustainable. This paper presents work performed in the first year of a project sponsored by the U.S. DOE GTO Waterless Stimulation Initiative that investigates foam fracturing as an alternative approach to hydraulic fracturing. One element of this work explores foam formulations that are suitable for EGS conditions. A separate paper submitted to this workshop covers the relevant work on foam characterization (Thakore et al., 2020).

This paper describes the development of an experimental setup for studying the applicability of foam fluids for hydraulic fracturing along with enhanced fracture efficiency through cyclic pressurization. The system is equipped with pulse rate automation, dual pulse valves for enhanced pulsation amplitudes, and other functions. It can perform static injection at a given pressurization rate, and pulsed injection at specified pulse size and rate. Both single-phase and foamed fluids can be used. Initial experimental results of foam fracturing using cement as a model material are reported. The observations from the experimental work will be presented and discussed.

1. INTRODUCTION

Foam fracturing is considered a potential approach to address water availability challenges with development of enhanced geothermal systems (EGS). Currently, EGS relies on using water for hydraulic stimulation to create the fracture network required for extraction of geothermal energy. One study of the use of water in geothermal plant development estimated that nearly 2 million gallons (1 gal = 0.00379 m^3) per MW will be required for EGS reservoir stimulation (Clark et al. 2011). To achieve the U.S. DOE goal of 60 GW of geothermal power generation by year 2050, 120 billion gallons of water would be needed for hydraulic stimulation if alternatives to hydraulic stimulation are not developed. This does not consider additional water needs for well construction such as drilling and cementing. The challenge of meeting resource needs for EGS well construction and completion is further compounded by the fact that the most promising potential EGS sources in the U.S. are mostly located in the regions where water stress[b] is high or extremely high (Blackwell et al., 2011; Freyman, 2014). Technology innovation is needed to overcome technical and non-technical barriers and to mitigate the upfront cost and risk with reservoir stimulation. This study focuses on the foam fracturing as part of U.S. DOE waterless stimulation initiative.

Foam is an immiscible mixture of liquid and gaseous phases that behaves quite differently from the single constituent phases. For example, the viscosity of foam can be many times that of single phases like water or gas, depending on the quality of foam (gas volumetric fraction in mixture). The tunable properties of foam have been shown to be extremely attractive to EGS reservoir engineering. The high viscosity can reduce fluid leakage, increase fracture width, and improve proppant transportation. It is compressible with high energy storage providing sustained driving force for fracture propagation. The gas has very high permeability to penetrate the stressed body to create more complete fractures. Generally, an optimal foam performance can be obtained when the quality is 70% or higher (Faroughi et al., 2018). The implication is that a substantial amount of water can be replaced by the gaseous phase and, therefore, the usage of water can be reduced accordingly.

Foam fracturing has been used on a very limited basis in oil and gas fields dating back to the 1970's, primarily in low pressure and low permeability formations, but continues to be a subject of research investigation with additional technical challenges related to EGS implementation. EGS reservoir conditions and lithologies are substantially different from those of oil and gas. The earth stresses and temperature are generally higher and prospective EGS reservoirs are typically composed of rocks such as granite which has higher

[b] Measures total annual water withdrawals (municipal, industrial and agricultural) expressed as a percentage of water available.

strength and orders of magnitude less permeability than the typical sedimentary rocks in deep conventional oil and gas reservoirs. The stability and stimulation effectiveness of foam fluids for these conditions is an open question along with additional concerns related to mitigation of induced seismicity. We have proposed to evaluate the stability and effectiveness of foamed fluids for EGS scenarios and use pulsed injection to address these challenges. This is a new concept with many potential advantages including more efficient and reduced water usage and improved control of reservoir seismicity. Some research considerations were given in Wang et al. (2019).

This paper describes recent work performed at ORNL to develop an experimental system for studying foam fracturing using cyclic pressurization. Cement was used as a model material in this process. In the following, experimental technique and test results will be presented along with the discussions.

2. EXPERIMENTAL TECHNIQUE

2.1 Test system

A pulsed foam injection test system was developed through multiple modifications of an existing test line. The current version of the test system, Figure 1, was configured with liquid, gas and foam sections:

- The main components of the liquid section are shown in the upper right portion of Figure 1, which included SC air-driven pump (PM1), pressure gauge (PG), Parker relief valve (RV), Vickers accumulator (AC1), Swagelok pressure regulator (PR1), and High Pressure (HiP) check valve (CK1).
- The gas section in the upper left portion of Figure 1 consisted of N_2 gas cylinder (GC), Air Liquid (AL) pressure regulator (PR2), diaphragm valve, and HiP check valve (CK2).
- The foam section consisted of HiP tee connector (TEE), HiP in-line filter (IF), Bronkhorst Coriolis flow meter (FM), HiP rupture disc (RD), Honeywell pressure sensor (PS), and two Swagelok on-off ball valves actuated pneumatically using solenoid valves (PV1, PV2), specimen valve (SV) and back-pressure regulator (BPR).

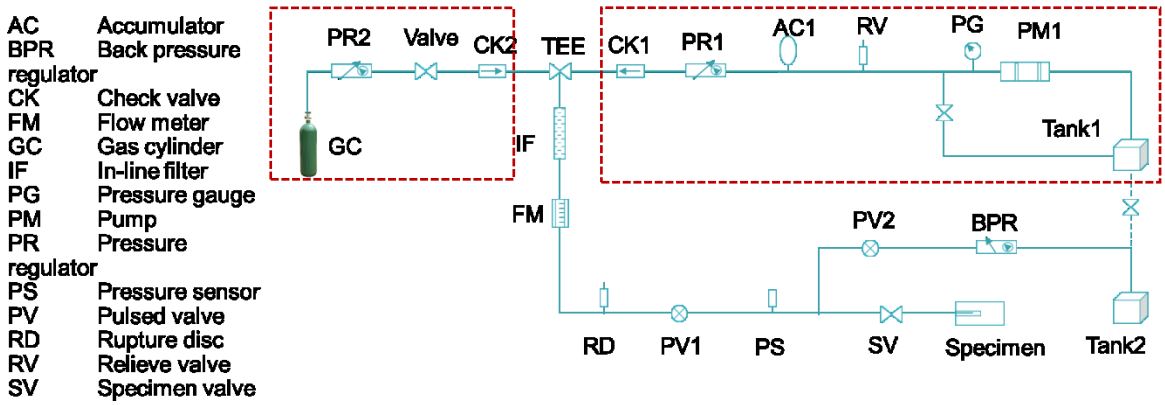

Figure 1: Diagram of test setup for foam fracturing study at ORNL. Tank1, PM1, AC1, PR1, CK1 are for the liquid line; CK2 is for gas line; PV1, PV2 and Tank2 are for foam line. The liquid and gas sections are outlined, respectively.

The system has serval unique features.

- A Bronkhorst FM measures the flow rate and density of fluid simultaneously. The density can be used to monitor the quality of foam. The quality is calculated from the mass balance equation $(\rho_l - \rho_{mix})/ (\rho_l - \rho_g)$. In this equation, the liquid density (ρ_l) and gas density (ρ_g) are given, and the mixture density (ρ_{mix}) can be read from the flow meter.
- Solenoid actuators for pneumatic valves are controlled by time-delay relay boxes. The timing for operation of pulsed valve(s) is implemented through the periods of pulse on (t_1) and pulse off (t_2) based on pulse settings. The pulse settings include: 1) pulse rate, $1/(t_1 + t_2)$; and 2) duty cycle, $t_1/(t_1+t_2)$. In pulsed injection, the opening and closing of pulsed valve(s) generates the required pulsation once the pre-determined pressure level is set up.
- The system can be configured with single pulse valve or dual pulse valves. The dual valves can be operated in an out-of-the-phase mode for enhanced pulse amplitude. Namely, PV1 is opened and PV2 is closed for pulse on, and vice versa for pulse off.

Cyclic stimulation has been used in EGS field development before (Zimmermann et al., 2010; Chabora and Zemach, 2013). These previous efforts controlled pumping operations at the surface with pressure cycling accomplished by intermittent fluid injection over periods of hours or days. The approach in this study is quite different in that high frequency pressure cycling is explored without cessation of pumping (i.e. pressure is cycled between a high- and low- pressure value). This functionality is accomplished by active control of flow valves and enables controlled exploration of the potential for stimulating rock failure by fatigue. The valves, tubing, fittings, sensors, gauges and regulators in the laboratory experimental setup for this study all have a pressure rating of at least 20.69 MPa, with exception for RD, PVs and BPR whose rated pressure is 13.79 MPa. The pulse rate can be varied from 0.5 to 5 Hz.

Foam production is accomplished by separate injection and metering of liquid and gas to produce the desired foam quality. The liquid phase is first injected at a controlled pressure range using PR1 and BPR. Gas is separately injected into the line to obtain the target foam quality and flow rate using PR2 and a gas metering valve. An in-line filter is used to promote mixing of gas and liquid phases and homogenize the foam mixture. In pulsed injection tests with foam, the solenoid valves controlling flow to the specimen and flow to the tank are energized once the foam quality and flow rate reached the target ranges. Manipulation of valves and flow rates for foam production was performed manually for the experiments reported in this paper with the exception of the pulsed injection solenoid valves. This proved to be very challenging to control as will be shown in 3.2. The system is currently in the process of being upgraded to enable automated control of foam quality.

A LabView program was employed to acquire the pressure data. The data communication between the sensors and the LabView program was established using a NI USB-6251 I/O device along with connection board SCB-65. The program has normal acquisition and rapid acquisition modes that can be used in static and pulsed test conditions. The sampling rate and number of data blocks or data points for each block can be set up as required. Meanwhile, Bronkhorst FlowPlot was used for DAQ on flow rate, fluid temperature, and density. A client server FlowDDE needs to be started to run the FlowPlot.

2.2 Materials

Cement was used as a test material to calibrate and refine the experimental system and to develop an understanding on the response of rock-like materials under target conditions. We have tested three cylindrical specimen sizes with the dimensions summarized in Table 1. The majority of the specimens in Table 1 were dedicated to static injection tests, while less than half of C2 and C3 series used in pulsed injection tests. Test samples were prepared at Temple University with a water to cement weight ratio of 1:1. These samples were cured in water the second day after being cast, removed from water after 28 days, and then transported to ORNL in various time periods. The samples were stored in air until specimen preparation and tests were conducted. The related information is provided in Table 1 as well. Six C1 samples were tested to evaluate the mechanical property, and the compressive strength was obtained as 56 ±4 MPa. In the following, prefix like "C1-" will be dropped off for simple description whenever it is possible.

All samples were internally pressurized through a blind borehole drilled to half-length of specimen. The same borehole diameter of 9.53 mm was used for all the specimens to simplify preparation. Use of the same borehole diameter resulted in various ratios of borehole diameter to cylinder diameter that slightly affected the fracturing response due to stress field differences. The use of a blind borehole specimen is similar to field stimulation conditions at the end of a borehole (Li et al., 2015; Wanniarachchi, et al., 2018). A 316 stainless steel (SS) 6.35 mm OD × 4.57 mm ID tube served as a fluid conduit to the borehole. The OD of the tube was bonded to the hole surface using high-strength epoxy DP420 (3M, 2019) and allowed to cure for at least 24 hours before testing to achieve full mechanical strength. Epoxy was not applied to the lower 6.35 mm of the tube, which was used as part of the pressurizing zone. The tube was also extended about 31.75 mm outside of the specimen for pressure fitting connection. Two O-rings were installed to prevent the epoxy from flowing to the bottom of the blind hole.

The length of bonding was selected to withstand pullout of the tube at a specified pressure level. For the test scenario, the shear resistance of the epoxy bond must be able to resist the force of the foam pressure on the projected area of the pressurization tube. Calculations were made to evaluate the interface shear strength at a pressure 13.7 MPa. The safety factor for the shortest specimens, the C2 series, was calculated to be 3.91.

Table 1 Cement specimens used in this study

Series	Spec. ID	Spec. diam. (mm)	Spec. length (mm)	Borehole diam. (mm)	Borehole depth (mm)	Note
C1	C1-01 to C1-06	50.80	101.60	9.53	50.80	Cast on Nov.2, 2018, immersed in water for curing on Nov. 3, 2018, and removed from water on Dec. 1, 2018; received and tested in Jan. 2019.
C2	C2-01 to C2-10, C2-A to C2-J	38.10	76.20	9.53	38.10	Cast on Nov.2, 2018, immersed in water for curing on Nov. 3, 2018, and removed from water on Dec. 1, 2018; received in Jan. 2019 and tested in May to Jul. 2019.
C3	C3-01 to C3-10	101.60	203.20	9.53	101.60	Cast on Mar. 4 or Mar. 5, 2019, cured in water the next day, and removed from water on Apr. 2 or Apr. 3, 2019; received in May 2019 and tested in May to Aug. 2019.

2.3 Foam

A range of candidate foams were studied for potential use in waterless stimulation of EGS. For this study, the primary candidates of interest were N_2-based foams. Experimental fracture testing to date has used N_2 as a gaseous phase at 70% quality with 0.4 wt.% alfa olefin sulfonate (AOS) as surfactant. The relevant properties of the foam can be found out in Thakore et al. (2020).

2.4 Test plan

The injection tests with water were conducted under pressure control mode. The tests were performed without confining pressure at room temperature (RT). The un-confining case was considered in this study mainly because of the simple implementation. This enables us to focus on development of the testing system and concept verification for the downhole foam injection. The graphs in Figure 2 illustrate the standard pressure profile used for static and pulsed injection tests.

For foam injection, the foam must be generated before the injection. In this study, the target flow rate and density of foam for fracturing were set at 10-30 ml/min and 300 kg/m^3. The former was close to the flow rate used in various laboratory studies on hydraulic fracturing and the latter was designed to deliver a foam quality of 70%.

2.4.1 Static injection

Tests in this mode is designed to be quasi-static such that the pressurizing rate, defined as P_{max}/T_{max}, has insignificant effect on data interpretation. Haimson and Fairhurst (1969) observed such effect in hydraulic fracturing of hydrostone specimens in the range of 0.04 to 1.14 MPa/s.

There is no official standard for static injection testing. The test plan for this study referred to ASTM D3967-16 standard, which applies to tensile strength testing of rock core specimens, for guidance. It requires a loading rate of between 0.05 and 0.35 MPa/s. This is consistent with prior laboratory and field testing experience. For example, in laboratory studies of Li et al. (2015) and Wanniarachchi, et al. (2018), the rate was set between 0.01 and 0.22 MPa/s. In the field (Valko and Economides, 1997), a pressurization rate 0.19 MPa/s is estimated considering a breakdown pressure of 45 MPa achieved in 40 min. Based on the above considerations, the loading rate criteria used for this study were a time the static pressure target not less than 1 min or pressurization rate not higher than 0.35 MPa/s in order to maintain quasi-static conditions.

2.4.2 Pulsed injection

Pulsed injection tests cyclically varied pressure values between a maximum pressure, P_{max}, and a minimum pressure, P_{min}, as shown in Figure 2(b) below. With the dual pulse vales, P_{min} can be as low as zero. In this study, tests were performed at 0.5 Hz pulse rate with 50% duty cycle. Given a pulse frequency, the pressure curve can be characterized using pressure amplitude,

$$P_a = (P_{max} - P_{min})/2, \quad (1)$$

and mean pressure,

$$P_m = (P_{max} + P_{min})/2. \quad (2)$$

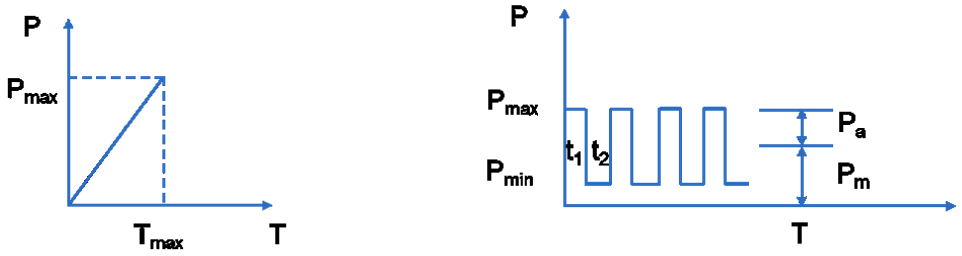

(a) (b)

Figure 2: Pressurization as a function of time for (a) static and (b) pulsed injection tests. In the latter, t1 and t2 define the pulse-on and pulse- off durations.

3. TEST RESULTS

3.1 Static injection with water

Most of the specimens were tested to failure. A few specimens were statically pressurized without failure at first and then re-tested to failure as follow-up tests. These specimens were still considered as static test case because the follow-up test pressures were lower than the previous max. pressure, including C2-06, and C3-03, C3-05. Typical static tests were completed in a range of 120 s to 1600 s as shown in Figure 3, with averaged pressurization rates from 0.005 to 0.1 MPa/s. Specimen failure consistently occurred in a plane perpendicular to the cylindrical axis as expected for this loading condition due to a stress concentration with a large tensile component

in the axial direction. This failure mode is related to the blind hole geometry and loading and has been reported in other relevant hydraulic fracture studies of rock (Li et al., 2015).

Static testing results for the three series of cement are summarized in Table 2. The max. pressure P_{max} or breakdown pressure varied among the three series. A couple of factors may contribute to the variation observed.

- Casting of cement may be affected by the mold. For example, C2 samples were prepared using a long PVC pipe with diameter 42.42 mm and length 304.80 mm as mold, and specimens were sectioned from the long cylindrical samples. Other two series were prepared using individual molds. A higher level of porosity can be seen on the outside surfaces of C2 specimens.
- The ratio of borehole to specimen diameter varied from 0.09 to 0.25. For the large borehole diameters of C1 and C2, the local stress in the bottom of borehole could be affected by the far field stress. We observed that the P_{max} of C1 was 7.28 MPa, about 13% of the compressive strength. Usually, tensile strength of material is used in comparison, while resolving of such tensile strength from breakdown pressure would require detailed numerical analysis.

Test data for some specimens was either flawed or inadequately captured during early experimental trials when optimal operating approaches were being developed (e.g. pressure overshoot or low data acquisition sampling rate occurred for specimens #3, 5 in C1, #1, 5, 7, 8 in C2, and #1 in C3). Some results were excluded because of internal flaws within the specimen that produced premature failure. In a couple of cases, the failure occurred well below the bottom of blind hole where pressurized fluid reached a large-size structural flaw.

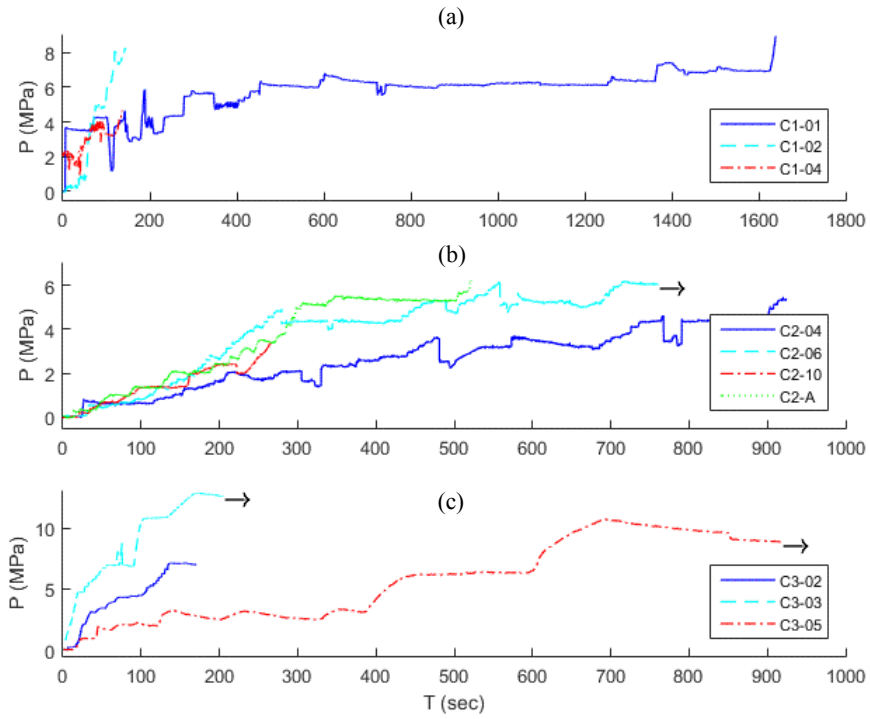

Figure 3: Hydraulic fracturing test results under static injection for (a) C1, (b) C2 and (c) C3. Arrow indicates that the test was stopped without specimen failure.

Table 2 Static tests of cement materials obtained with water as fracturing fluid

Series	Fluid	Spec. diam. (mm)	Borehole diam. (mm)	P_{max}, mean (MPa)	P_{max}, std. (MPa)	# of spec.
C2	Water	38.10	9.53	5.32	1.17	4
C1	Water	50.80	9.53	7.28	1.88	3
C3	Water	101.60	9.53	10.24	2.36	3

3.2 Static injection with foam

Foam fracturing tests were conducted under static injection for the C3 series, including C3-03-2, C3-05-2, C3-07-2, C3-08, C3-09. Those with suffix -2 are the specimens that were tested previously with water but not to failure as mentioned in Section 3.1. For instance, C3-05, which was initially tested with water, was renamed as C3-05-2 after being tested with foam. A representative set of data is given in Figure 4 for C3-05-2. As discussed, the targets for flow rate and density of foam were 10- 30 ml/min. and 300 kg/m^3, respectively. During the test, they responded promptly to adjustments made with the PRs and BPR in liquid and gas sections. The mean values and intervals (one std.) of these quantities were 53 ± 72 ml/min, and 440 ± 328 kg/m^3, respectively. The specimen fractured at 7.03 MPa; foam conditions at specimen failure were 30 ml/min and 300 kg/m^3. As can be seen, the test took a relatively long time to finish. This was due to the difficulty of controlling foam quality manually as explained in section 2.1.

Test results for C3 series specimens fractured with foam are given in Table 3 in terms of foam parameters and breakdown pressures. Two specimens are not included in this table. The failure pressure of C3-08 was not captured due to a rapid pressure build-up and inadequate data acquisition sampling rate. Specimen C3-09 appeared with premature failure due to a large internal flaw.

The behavior of C3-07-02 is consistent with prior foam fracturing studies in oil and gas application that have shown breakdown pressure using foam to be slightly greater than that using water (Valko and Economides, 1997; Wanniarachchi, et al., 2018). Failure of two samples in Table 3 occurred at pressures below maximum levels experienced during prior static injection trials with water. These results cannot be conclusively explained but it is suspected that they could be due to fatigue damage experienced by the samples over the course of loading or increased pressure in permeable cement zones near the blind hole due to the higher viscosity of the foam.

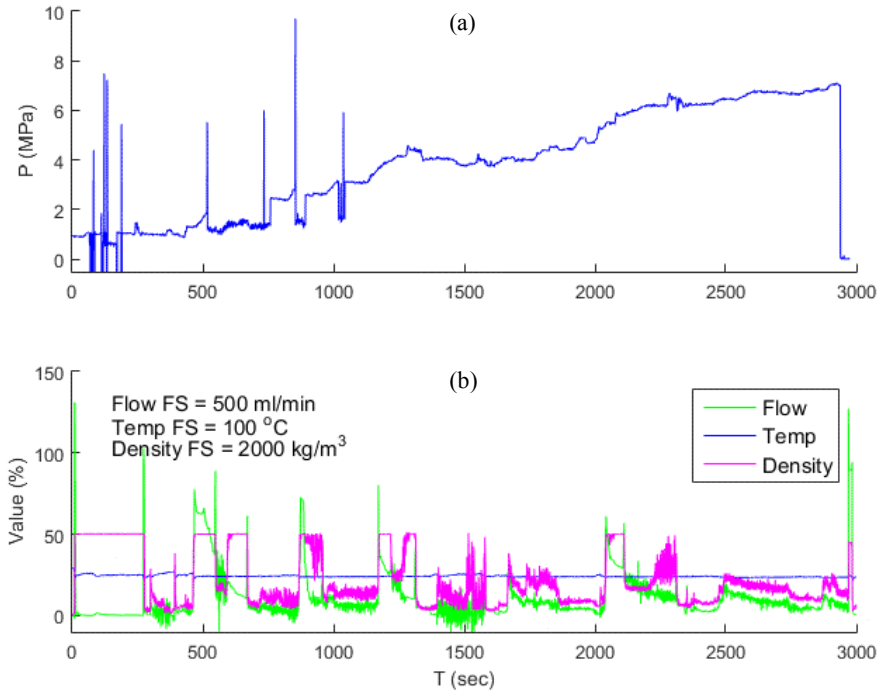

Figure 4: Foam fracturing results of C3-05-2, tested w/o failure using water and re-tested using N_2 foam: (a) pressure curve, (b) flow rate, temperature and density; FS – full scale.

Table 3 Specimen and N_2 foam conditions of C3 cement in static injection tests

Spec.	Previous max. pressure w/ water (MPa)	Flow, mean (ml/min)	Flow, std. (ml/min)	Density, mean (Kg/m^3)	Density, std. (Kg/m^3)	Flow at failure (ml/min)	Density at spec. failure (Kg/m^3)	Breakdown pressure w/ foam (MPa)
C3-03-2	12.88	57	86	482	416	18	100	5.24
C3-05-2	10.69	53	72	440	328	30	300	7.03
C3-07-2	7.23	63	79	366	316	45	320	11.07

3.3 Pulsed injection

The specimens in this condition were largely tested using dual valves system, while a couple of specimens C2-03 and C2-09 tested using single-valve system. The PV2 in dual valves can help the system to build up pressure in pulse on and discharge in pulse off more effectively, which would be depending on BPR if a single pulse valve is used. However, use of the different systems should not have any significance effect on the characterization of material response because we quantified the input using mean pressure P_m and pressure amplitude P_a as shown in Figure 2. Two pressure cycling results are shown in Figure 5 for C2-C and C2-D, in which a segment of pressure profile is also presented for C2-C showing how the pulsation has been implemented. These plots represent extreme cases with relatively low and high fatigue lives at respective pulse levels. In C2-C, the initial value of P_{max} was approximately 1 MPa and was reduced when the pressure could not be applied as designed because of the imminent failure. In the case of C2-D, the pulsed injection lasted about 10,000 s with some adjustments of pulse size and pulse level during the process. The large difference in fatigue life for the two specimens was shown to be related to the strength-limiting flaws in addition to pulsed pressure levels.

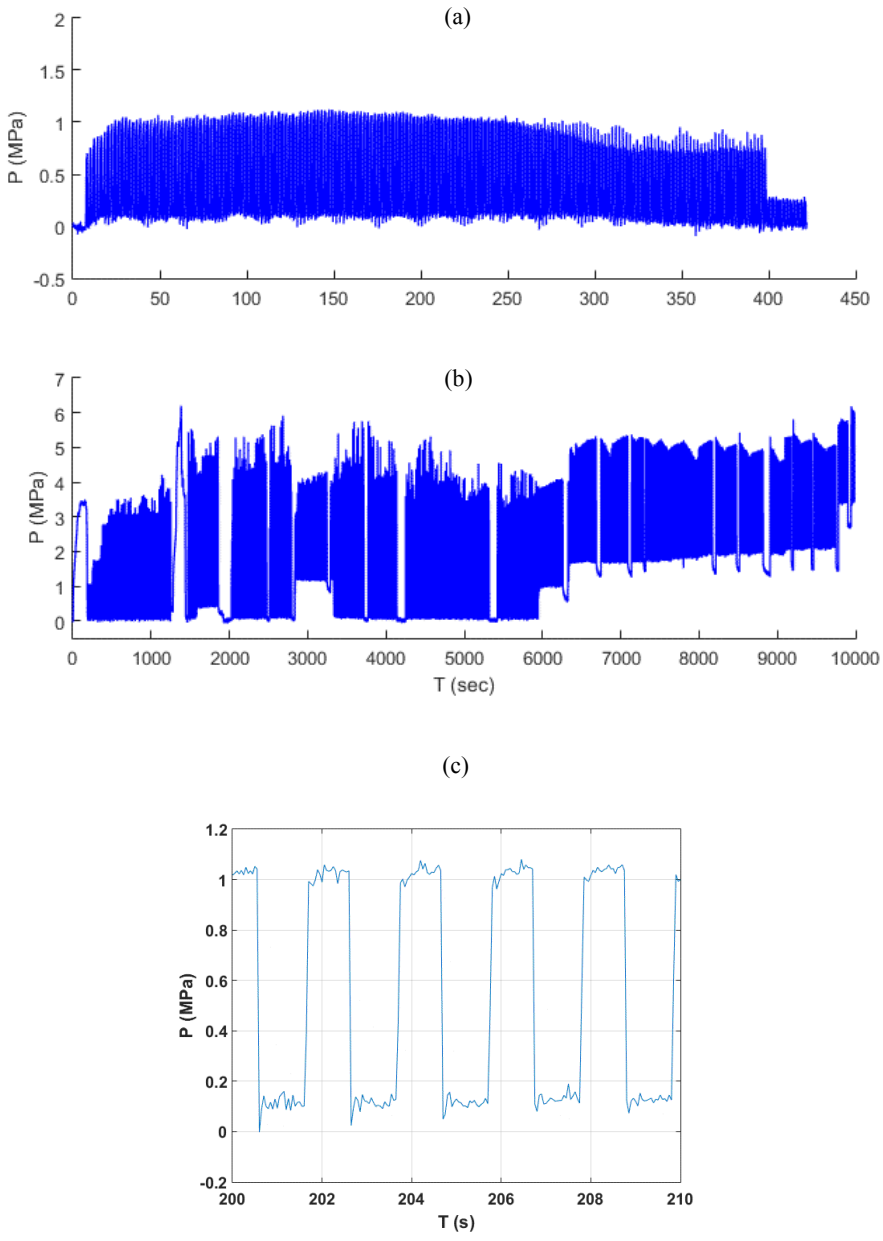

Figure 5: Hydraulic fracturing results under pulsed injection for (a) C2-C, (b) C2-D, and (c) a segment of pressure profile taken from C2-C showing five cycles of pulse.

Pulsed injection test results are shown in Figure 6 in terms of pressure amplitude versus the number of cycles to failure. The number of pressure cycles was estimated based on the test time and pulse rate. Fatigue life varied widely as can be seen from data points of series C2 even for the same pulsed pressure condition. This is likely due to structural differences in the samples and will be discussed in more detail in section 4.

Pulsed injection was also conducted using the N_2 foam. However, we only obtained one data point on C3-10, and that is illustrated in Figure 6 as well. The pulsed injection of foam was carried out by energizing the pulse valves once the pre-determined foam condition was established. More work is apparently needed in order to characterize the response of the material under this condition.

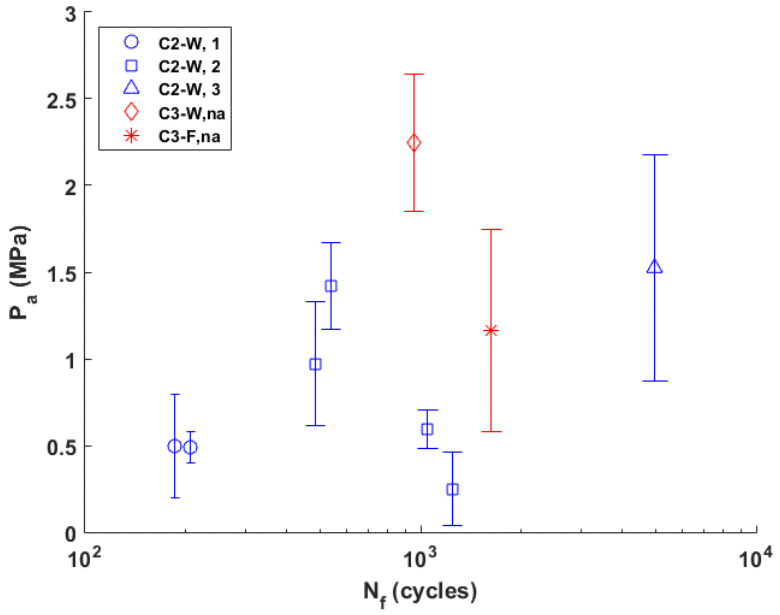

Figure 6: Pressure amplitude as a function of number of cycles to failure for C2 and C3, under pulsed injection; error bar corresponds to one standard deviation. Legend 'XX-Y, Z' is designated as follows: XX- cement series, Y- water (W) or foam (F), Z- flaw type.

4. DISCUSSION

4.1 Fracture completeness

The fracture induced by foam is more complete than that produced by water. The terminology "complete fracture" was used in some previous work such as that of Wanniarachchi et al. (2018). It describes a type of failure in which the material is completely fractured into small pieces, such as in foam fracturing. It is used because some incomplete fracture occurs where the failed specimen still maintains the original geometrical shape with bridges existing between fractures. We introduce fracture completeness to quantify the response of material, namely, ratio of the number of specimens with complete fracture to the total number of specimens tested. The results showed, only 50% fracture completeness was obtained for the 24 specimens fractured using water, whilst for the specimens fractured with foam (8), 100% was achieved. This is a very important because it means a more effective fracture network could be created with foam, and therefore, the permeability would be enhanced as desired. Apparently, the effect of surrounding rock mass and confining pressure on characteristics of foam fracturing remains to be studied. The high fracture completeness rate with foam fracturing is believed to be attributed to the high permeability of gaseous phase (Wanniarachchi et al., 2018). Upon the creation of additional cavity space, the volume expansion would result in the breakdown of foam and release of N_2. The gas can deliver the pressurization effectively to rest of the body that can be stressed more evenly than using water.

4.2 Failure mode

Fracture plane orientations for specimens occurred either 1) perpendicular to the cylinder axis (transverse fracture), or 2) perpendicular to the base of the cylinder (axial split). For the 14 specimens analyzed, statistics indicated that 71% sample failures were of the transverse fracture type and the rest were of the axial split type. When the pressurization was nominally contained with the blind hole section as designed, failure usually took the form of transverse fracture near the end of the hole. This is consistent with the stress concentration produced by the hole configuration and loading conditions as described previously. Example traverse fracture images are provided in Figure 7 for specimen C3-05-2. Pre-existing surface cracks were visible as delineated by black marker in the left image. The surface cracks are believed to be caused by the shrinkage related to hardening. However, the fracture of specimen was initiated from the inside borehole and did not follow the surface cracks.

Normally, the gap between SS tube and hole surface is filled completely by epoxy to have a good bonding as discussed in 2.2. But this was not always the case; for some specimens, a cavity was formed because the gap was not fully filled. The pressurized fluid penetrated the inside and outside interfaces of the O-ring into the cavity, and equivalently, extended the pressurization length. The hoop stress of thick-walled cylinder obviously increases with the increasing pressurization length, which will overtake the axial stress at some point of time to trigger the fractur in axial direction. This can be seen from the estimates of the pressurization length ratio (PLR) to the depth of borehole. The PLR was 0.25 ± 0.07 for 10 specimens dominated by transverse fracture and increased to 0.59 ± 0.09 for 4 specimens dominated by axial split.

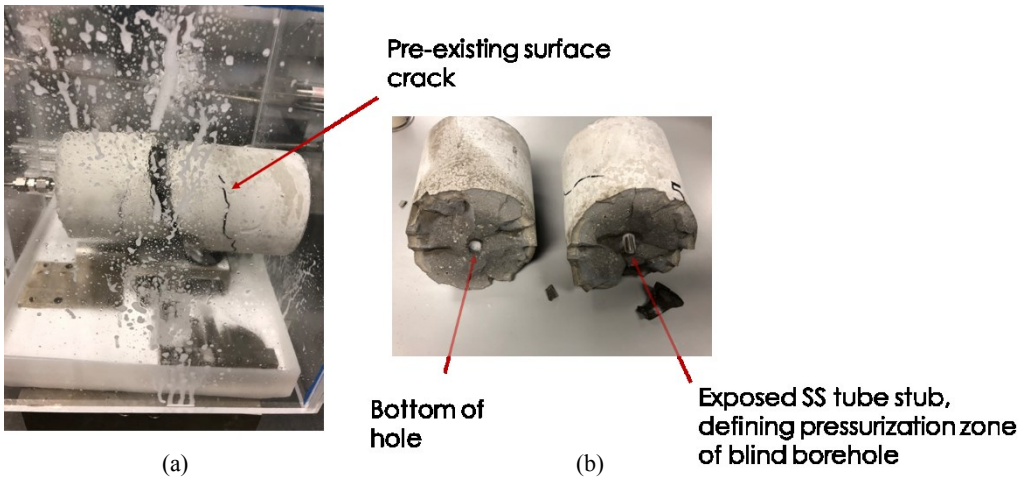

Figure 7: Failure of C3-05-2 generated by foam fracturing, dominated by transverse fracture: (a) specimen at failure, (b) fracture surface of mating halves.

4.3 Structural flaws

Given failure mode as described, the failure of materials would be dominated finally by structural flaws. For the pulsed injection tests, let's consider C2 series that had a good number of samples for the analysis. The fractography revealed roughly three types of flaws.

1) Flaws that have large size and are located near the hole surface or within the wall, such as in C2-C. The flaws were agglomerates or pores resulting from material fabrication, and large enough to impose substantial effect on the load bearing area.
2) Porous regions or pores in small scale near the hole surface such as that in C2-B, which may be from fabrication.
3) Machining flaws in microscale from hole preparation like drilling of borehole such as that in C2-D.

Figure 8 shows the pictures of the three types of flaws. Generally, the inner half-radius region of fracture surface was relatively smooth with intersecting facets in various orientation. The outer half-radius region was rough, consisting of ridges and valleys. Failure origin can be found out on the borehole surface, which may be located on the wall of borehole or near the corner of bottom. Pore, porous region, agglomerate, and machining crack was observed as fracture initiation site. Further image analysis is needed to quantify structural flaws in future.

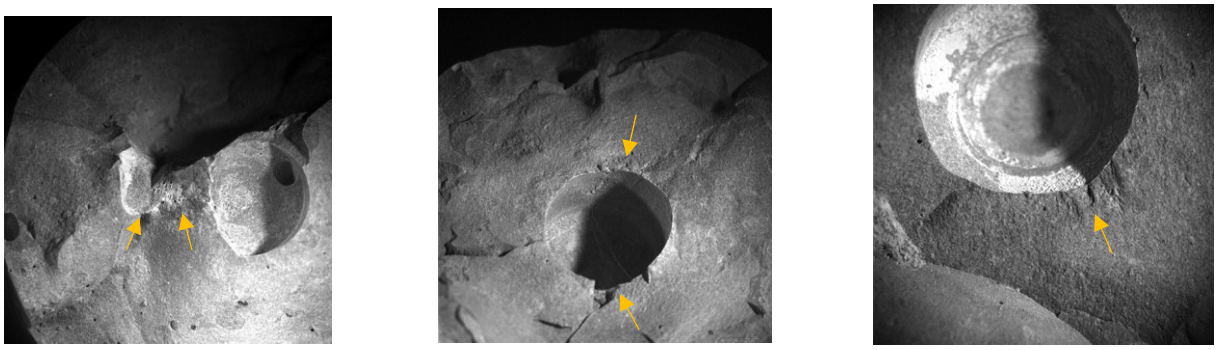

Figure 8: Failure mechanisms are controlled by structural flaws: (a) large size agglomerate in C2-C, ×7.5, (b) porous region and triple area (missing) in C2-B, ×7.5, and (c) machining flaw in C2-D, ×15. Arrows indicate the flaws identified near the borehole.

In the case of machining crack as only type of strength-limiting flaws, the lifetime of material was relatively long. The involvement of the flaws like types 1 and 2 tends to shorten the lifetime as can be seen from flaw-based P_a vs. N_f plot in Figure 6.

4.4 Fatigue failure considerations

The results of pulsed injection tests on C2 with type 2 structural flaws (as defined above) are presented in Figure 9 on a constant fatigue life diagram. The data point on horizontal axis corresponds to the breakdown pressure P_{max} from static tests (without pulsation). All the pulsed data points are seen falling in the triangular area defined by $P_a = P_m$ and $P_a + P_m = P_{max}$. Moreover, the number of cycles to failure appears to exhibit a dependence on pressure amplitude P_a and mean pressure P_m.

Therefore, if flaws in the material are present, hydraulic fracturing using pulsed injection can produce fracture growth at pressure levels ($P_m + P_a$) lower than the breakdown pressure for static injection. If similar behavior is shown to apply to naturally fractured rock, then this diagram may be useful for informing fracturing job design using pulsed injection.

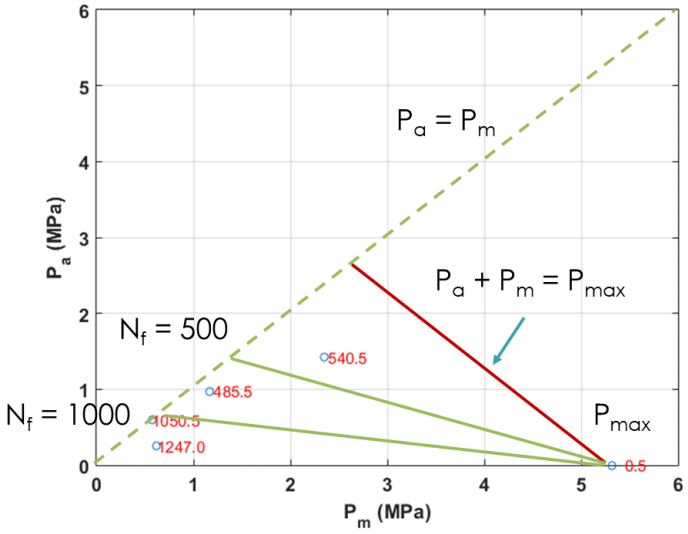

Figure 9: Constant fatigue life diagram based on pulsed injection test results of C2 series with water as fracturing fluid; label next to each data point is fatigue life in cycles; lines are drawn for illustration.

5. CONCLUSIONS

A foam injection testing system has been developed with both static and pulsed injection functionalities. Using cement as a test material, pulsed and foam injections have been demonstrated on blind borehole cylindrical specimens. Test results were obtained for both injection modes with water and N_2 foam as fracturing fluids. While the current experimental sample set is small, three observations are made from the data produced during testing and post-test examination of specimens:

- Breakdown pressure for static injection tests increased with a decrease of borehole diameter to specimen diameter ratio.
- The use of foam for pressurization produced more extensive damage to specimens than water alone.
- Hydraulic fracturing using pulsed injection can produce sample failure at pressure levels ($P_m + P_a$) lower than the breakdown pressure needed for static injection pressurization.

The last observation has intriguing possibilities for increasing formation fragmentation and permeability when natural fractures or other flaws are present. The ability to rapidly cycle applied pressure during stimulation remains a challenge for field application, but if suitable downhole technology can be developed for the implementation of the technique, then the possibility exists to take advantage of fatigue behavior to perform more effective hydraulic reservoir stimulation. It should be noted that the effect of pulsed injection on the number of cycles to failure would be depend on the other pulse settings like pulse rate, and environmental conditions like confining pressure. The current testing and characterization focused on the pressure amplitude and mean pressure for pulse settings and un-confined condition at RT. The effectiveness of pulsed injection would be evaluated once the data of fatigue responses are obtained under these target conditions.

Future work will be focused on the following:

- Injection testing system development will be upgraded for higher pressure rating (41.37 MPa) and better flow/ injection control.
- Foam fracturing tests will be continued on rock/ granite specimens with blind and open borehole configurations.
- Experimental methods for heating and applying confining pressures will be explored for the injection testing system.

- Stability study on N_2-in-water and CO_2-in-water foams will be continued, including four surfactants and three types of gelling agents. Foam drainage data will be collected between RT and 200^oC.

ACKNOWLEDGMENTS

This research was sponsored by the US Department of Energy, Assistant Secretary for Energy Efficiency and Renewable Energy, Geothermal Technologies Office, as part of the Enhanced Geothermal Systems Program under Contract No. DE-AC05-00OR22725 with the US Department of Energy.

Authors are grateful to Anthony McBee, Danny Parrott of ORNL for their help in building time delay relay box, Randy Parten of ORNL for preparing specimens, Harmon Phillips of Control Management Technology, Carmen Bracco of TEK CV&F, Larry Miller of Airgas for their help and discussion on fluid measurement and control. Authors also thank Drs. Lianshan Lin and Michael Lance of ORNL for reviewing this manuscript.

REFERENCES

3M: Scotch-Weld, Epoxy Adhesive DP420 Black, DP420 NS Black, DP420 Off-White, DP420 LH, Technical Data, Apr. 2019, www.3M.com/structuraladhesives.

ASTM D3967-16 Standard Test Method for Splitting Tensile Strength of Intact Rock Core Specimens, ASTM International, West Conshohocken, PA 19428, Nov. 2016.

Clark, C.E., Harto, C.B., Sullivan, J.L., Wang, M.Q.: Water Use in the Development and Operation of Geothermal Power Plants, ANL/EVS/R-10/5, Jan. 2011

Chabora, E., Zemach, E.: Desert Peak EGS Project, Geothermal Technologies Program 2013 Peer Review, U.S. DOE EERE, Apr. 22, 2013.

Faroughi, S.A., Pruvot, A.J.-C.J., and McAndrew, J.: The Rheological Behavior of Energized Fluids and Foams with Application to Hydraulic Fracturing: Review, *J. of Petroleum Sci. and Eng.*, **163**, (2018), 243-263.

Freyman, M.: Hydraulic Fracture & Water Stress: Water Demand by the Numbers, Ceres, Feb. 2014.

Haimson, B., Fairhurst, C.: 1969, Hydraulic Fracturing in Porous-Permeable Materials. *J. of Petroleum Tech.*, July 1969: 811-817.

Li, X., Feng, Z, Han, G., Elsworth, D., Marone, C., Saffer, D.: Hydraulic Fracturing in Shale with H_2O, CO_2 and N_2, The 49th US Rock Mechanics / Geomechanics Symposium, San Francisco, CA, USA, July 1, 2015, ARMA 15-786.

U.S. DOE: GeoVision, Harnessing the Heat Beneath Our Feet, 2019, https://www.energy.gov/eere/geothermal/downloads/geovision-harnessing-heat-beneath-our-feet, accessed Jan. 2020.

Valko, P. and Economides, M.J.: Hydraulic Fracture Mechanics, New York: John Wiley & Sons (1997).

Thakore, V., Ren, F., Voytek, J., Xi, J., Wang, H., Wang, J.-A. J., Polsky, Y.: High-Temperature Stability of Aqueous Foams as Potential Waterless Hydrofracking Media for Enhanced Geothermal Systems (EGS), *Proceedings*, 45th Workshop on Geothermal Reservoir Eng., Stanford U., Stanford, CA, Feb. 10-12, 2020, SGP-TR-216, 535-544.

Wang, H., Wang, J.-A.J., Polsky, Y., Ren, F.: Research Considerations for Foam Fracturing in Stimulation Development for Enhanced Geothermal Systems, *Proceedings,* 44th Workshop Geotherm. Reservoir Eng., Stanford U., Stanford, CA, Feb. 11-13, 2019, SGP-TR-214, 617-627.

Wanniarachchi, W.A.M., Ranjith, P.G., Perera, M.S.A., Rathnaweera, T.D., Zhang, D.C., Zhang, C.: Investigation of Effects of Fracturing Fluid on Hydraulic Fracturing and Fracture Permeability of Reservoir Rocks: An Experimental Study Using Water and Foam Fracturing, *Eng. Fract. Mech.*, **194**, (2018), 117-135.

Zimmermann, G., Moeck, I., Blöcher, G.: Cyclic Waterfrac Stimulation to Develop an Enhanced Geothermal System (EGS)—Conceptual Design and Experimental Results, *Geothermics,* **39**, (2010) 59–69.